

# **DEVELOPMENT OF A BENCHMARK EXAMPLE FOR DELAMINATION FATIGUE GROWTH PREDICTION**

Ronald Krueger

## **ABSTRACT**

The development of a benchmark example for cyclic delamination growth prediction is presented and demonstrated for a commercial code. The example is based on a finite element model of a Double Cantilever Beam (DCB) specimen, which is independent of the analysis software used and allows the assessment of the delamination growth prediction capabilities in commercial finite element codes. First, the benchmark result was created for the specimen. Second, starting from an initially straight front, the delamination was allowed to grow under cyclic loading in a finite element model of a commercial code. The number of cycles to delamination onset and the number of cycles during stable delamination growth for each growth increment were obtained from the analysis. In general, good agreement between the results obtained from the growth analysis and the benchmark results could be achieved by selecting the appropriate input parameters. Overall, the results are encouraging but further assessment for mixed-mode delamination is required.

## **INTRODUCTION**

Over the past two decades, the use of fracture mechanics has become common practice to characterize the onset and growth of delaminations. In order to predict delamination onset or growth, the calculated strain energy release rate components are compared to interlaminar fracture toughness properties measured over a range from pure mode I loading to pure mode II loading.

---

\*R. Krueger, National Institute of Aerospace, 100 Exploration Way, Hampton, VA, 23666, resident at Durability, Damage Tolerance and Reliability Branch, MS 188E, NASA Langley Research Center, Hampton, VA, 23681, USA.

The virtual crack closure technique (VCCT) is widely used for computing energy release rates based on results from continuum (2D) and solid (3D) finite element (FE) analyses and to supply the mode separation required when using the mixed-mode fracture criterion [1, 2]. The virtual crack closure technique was recently implemented into several commercial finite element codes. As new methods for analyzing composite delamination are incorporated into finite element codes, the need for comparison and benchmarking becomes important since each code requires specific input parameters unique to its implementation.

An approach for assessing the delamination propagation capabilities in commercial finite element codes under static loading was recently presented and demonstrated for VCCT for ABAQUS® [3]. In this recent paper, benchmark results were created for full three-dimensional finite element models of the Double Cantilever Beam (DCB) and the Single Leg Bending (SLB) specimen. Then, starting from an initially straight front, the delamination was allowed to propagate in the finite element model. The load-displacement relationship and the total strain energy obtained from the propagation analysis results and the benchmark results were compared and good agreements could be achieved by selecting the appropriate input parameters. Overall, the results were encouraging but it was determined that further assessment for mixed-mode delamination is required [3].

The objective of the present study was to create a benchmark example, independent of the analysis software used, which allows the assessment of the delamination fatigue growth prediction capabilities in commercial finite element codes. At the beginning, a benchmark example is created based on incremental finite element models of a DCB specimen. To avoid unnecessary complications, experimental anomalies such as fiber bridging were not addressed. First, a sample material and cyclic loading was selected. Second, the number of cycles to delamination onset,  $N_D$ , was calculated from the mode I fatigue delamination growth onset data of the material. Third, the number of cycles during stable delamination growth,  $\Delta N_G$ , was obtained incrementally from the material data for mode I fatigue delamination propagation by using growth increments of  $\Delta a = 0.1$  mm. Fourth, the total number of growth cycles,  $N_G$ , was calculated by summing over the increments  $\Delta N_G$ . Fifth, the corresponding delamination length,  $a$ , was calculated by summing over the growth increments  $\Delta a$ . Finally, for the benchmark case where results for delamination onset and growth were combined, the delamination length,  $a$ , was calculated and plotted versus an increasing total number of load cycles  $N_T = N_D + N_G$ . After creating the benchmark, the approach was demonstrated for the commercial finite element code ABAQUS®. Starting from an initially straight front, the delamination was allowed to grow based on the algorithms implemented into the commercial finite element software. Input control parameters were varied to study the effect on the computed delamination increase during cyclic loading. It was assumed that delamination length increase during cyclic loading obtained from finite element analysis should closely match the growth shown in the benchmark example. The benchmark enabled the selection of the appropriate input parameters that yielded good agreement between the results obtained from the growth analysis and the benchmark results. Once the parameters have been identified, they may then be used with confidence to model delamination growth for more complex configurations.

## METHODOLOGY

The methodology for delamination propagation, onset and growth [4] was applied to the DCB specimen (as shown in Figure 1) to create the benchmark example. Since the required material property input data were not readily available in the open literature for a single material, a fictitious set of properties was constructed for this benchmarking exercise. Individual properties for commonly used graphite/epoxy tape materials were obtained from the open literature to create this set to represent a typical graphite epoxy composite. The material properties are given in Table I.

### Static Fracture Toughness

The mode I fracture toughness (mixed-mode ratio  $G_{II}/G_T=0$ ) is generated experimentally using the DCB tests (as shown in Figure 1) [5]. A fracture toughness  $G_{Ic}=0.17 \text{ kJ/m}^2$  was used in this benchmarking exercise [6].

### Fatigue Delamination Growth Onset

The number of cycles to delamination onset,  $N_D$ , can be obtained from the delamination onset curve plotted in Figure 2 [7, 8]. The onset curve (solid green line) is a power law fit

$$G = m_0 \cdot N_D^{m_1} \quad (1)$$

of the experimental data (open, green circles) obtained from a DCB test using the respective standard for delamination growth onset [7].

An example of an applied energy release  $G_{max}=0.1362 \text{ kJ/m}^2$  resulting in  $N_D=150$  cycles to delamination onset was included in Figure 2 (dashed red lines). The significance of the data will be discussed later.

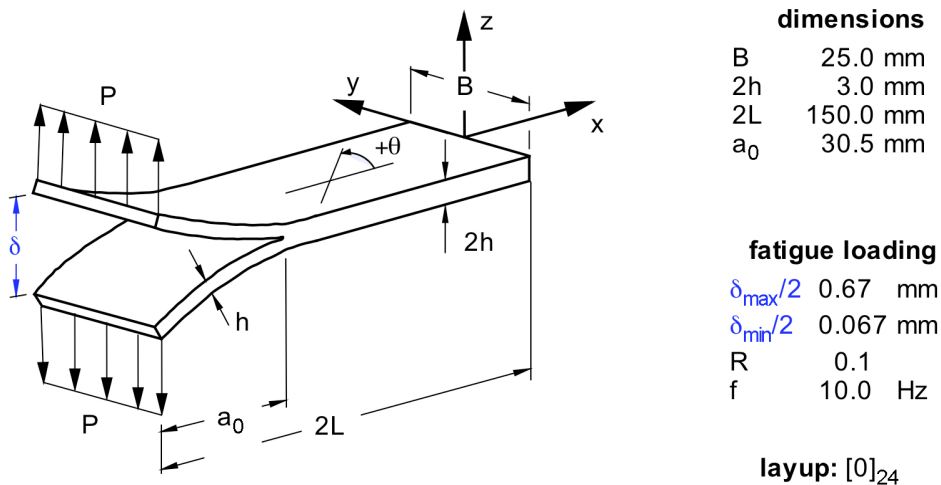


Figure 1. Double Cantilever Beam Specimen (DCB).

TABLE I. MATERIAL PROPERTIES

Unidirectional Graphite/Epoxy Prepreg [3]		
$E_{11} = 139.4 \text{ GPa}$	$E_{22} = 10.16 \text{ GPa}$	$E_{33} = 10.16 \text{ GPa}$
$\nu_{12} = 0.30$	$\nu_{13} = 0.30$	$\nu_{23} = 0.436$
$G_{12} = 4.6 \text{ GPa}$	$G_{13} = 4.6 \text{ GPa}$	$G_{23} = 3.54 \text{ GPa}$
Fracture Toughness Data [3]		
$G_{Ic} = 0.17 \text{ kJ/m}^2$	$G_{IIc} = G_{IIIc} = 0.49 \text{ kJ/m}^2$	$\eta = 1.62$
Delamination Growth Onset Data [8] – Figure 2		
$m_0 = -0.2023$	$m_1 = -0.078924$	
Delamination Growth Rate Data (Paris Law) [6] – Figure 3		
$G_{Ic} = 0.17 \text{ kJ/m}^2$	$G_{th} = 0.06 \text{ kJ/m}^2$	
$c = 2.44 \cdot 10^6$	$n = 10.61$	

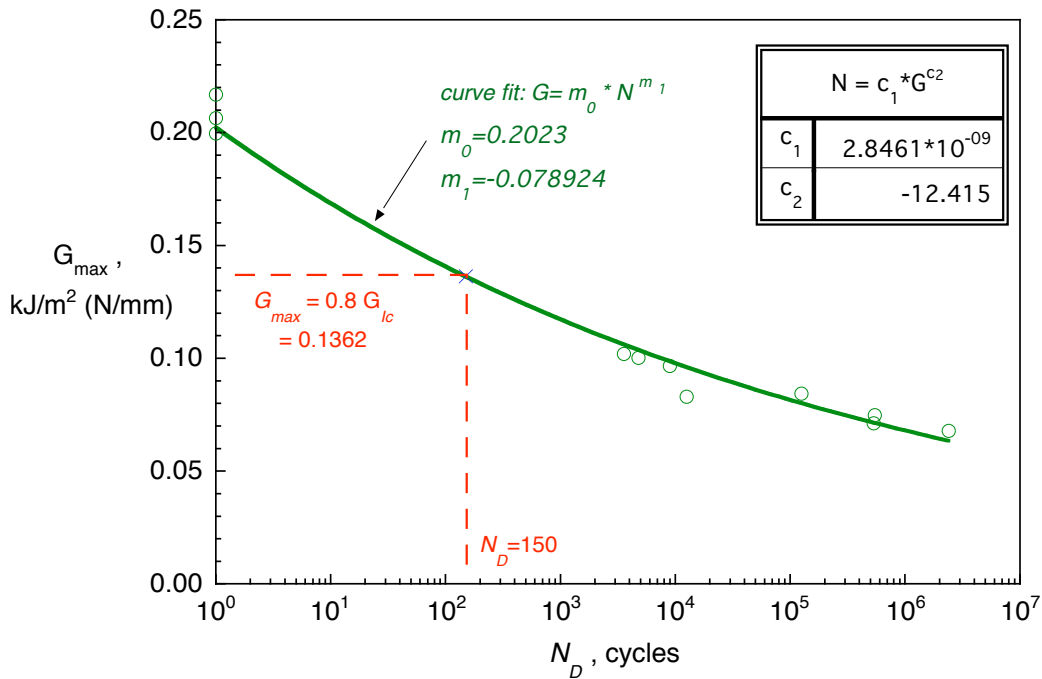


Figure 2. Delamination growth onset for DCB specimen.

## Fatigue Delamination Growth

The number of cycles during stable delamination growth,  $N_G$ , can be obtained from the fatigue delamination propagation relationship (Paris Law) plotted in Figure 3 [6]. The delamination growth rate (solid purple line) can be expressed as a power law function

$$\frac{da}{dN} = c \cdot G_{\max}^n \quad (2)$$

where  $da/dN$  is the increase in delamination length per cycle and  $G_{\max}$  is the maximum energy release rate at the front at peak loading. The factor  $c$  and exponent  $n$  are obtained by fitting the curve to the experimental data (open black circles) obtained from DCB tests [6]. The critical energy release rate or fracture toughness,  $G_{Ic}$ , was included in the plot of Figure 3 (blue solid vertical line). Since composites do not exhibit the same threshold behavior commonly observed in metals, a cutoff value,  $G_{th}$ , was chosen below which delamination growth was assumed to stop (green solid vertical line) [6]. This benchmarking exercise ignores branching or fiber bridging and hence the Paris Law was not normalized with the static R-curve.

An example of an applied energy release  $G_{\max} = 0.8 G_{Ic}$  was included in Figure 3 (red square). The significance of the data and the red arrow will be discussed later.

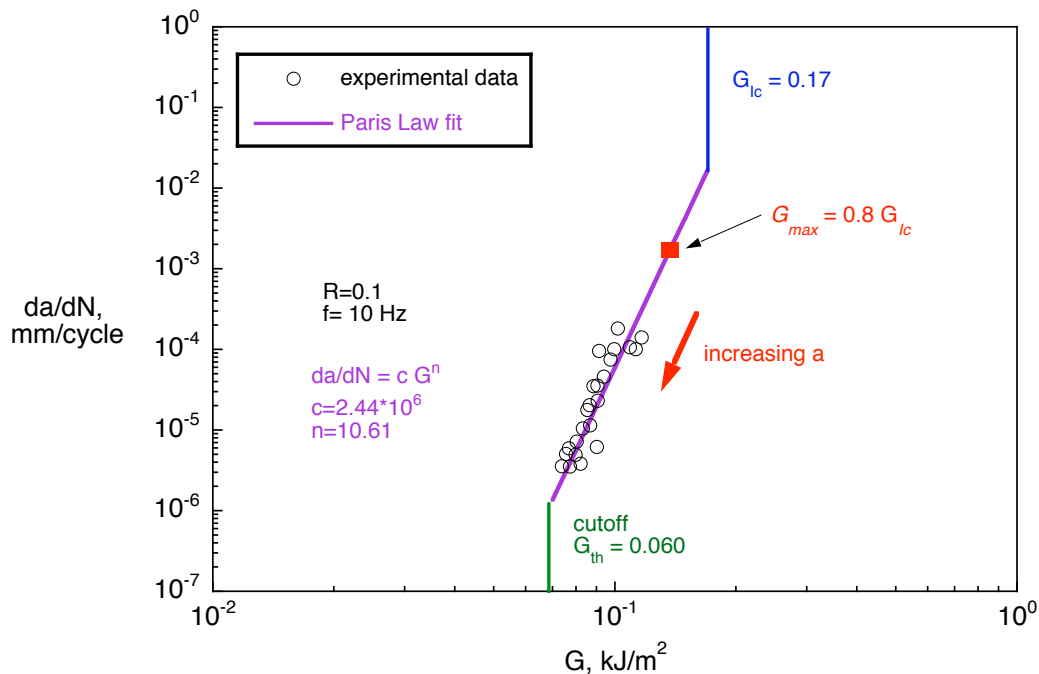


Figure 3. Delamination growth rate (Paris Law).

## SPECIMEN AND FATIGUE TEST DESCRIPTION

For the current numerical investigation, the Double Cantilever Beam (DCB) specimen, as shown in Figure 1, was chosen since it is simple, only exhibits the mode I opening fracture mode and had been used previously to develop an approach to assess the quasi-static delamination propagation simulation capabilities in commercial finite element codes [3]. To avoid unnecessary complications, experimental anomalies such as fiber bridging were not addressed. For the current study, a DCB specimen made of graphite/epoxy with an unidirectional layup,  $[0]_{24}$ , was modeled. The material properties are given in Table I. The material, layup, overall specimen dimensions including initial crack length,  $a$ , were identical to the specimen used earlier [3].

For the cyclic loading of the specimen, guidance was taken from a draft standard, where it is recommended to start the test at a maximum displacement,  $\delta_{max}$ , which causes the energy release rate at the front,  $G_{Imax}$ , to reach initially about 80% of  $G_{Ic}$ . The details are discussed in reference 6.

$$\frac{G_{Imax}}{G_{Ic}} = 0.8 \quad (3)$$

The maximum load,  $P_{max}$ , and maximum displacement,  $\delta_{max}/2$ , were calculated using the known quadratic relationship between energy release rate and applied load or displacement

$$\frac{G_{Imax}}{G_{Ic}} = \frac{P_{max}^2}{P_{crit}^2} \Rightarrow P_{max} = P_{crit} \sqrt{\frac{G_{Imax}}{G_{Ic}}}, \quad \delta_{max} = \delta_{crit} \sqrt{\frac{G_{Imax}}{G_{Ic}}} \quad (4)$$

$$\delta_{max} = \delta_{crit} \sqrt{0.8} \quad (5)$$

where  $P_{crit}$  and  $\delta_{crit}$  are the critical values. For the current study, a critical energy release rate  $G_{Ic}=0.17$  kJ/m<sup>2</sup> was used and the critical values  $P_{crit}$  and  $\delta_{crit}$  (grey dashed lines) were obtained from the benchmark for static delamination propagation [3] shown in the load-displacement plot in Figure 4. The calculated maximum load,  $P_{max}$ , and calculated maximum displacement,  $\delta_{max}/2$ , are shown in Figure 4 (dashed red line) in relationship to the static benchmark case (solid grey circles and dashed grey line) mentioned above. During constant amplitude cyclic loading of a DCB specimen under displacement control, the applied maximum displacement,  $\delta_{max}/2=0.67$  mm, is kept constant while the load drops as the delamination length increases (solid red circles and solid red line). The energy release rate corresponding to an applied maximum displacement  $\delta_{max}/2=0.67$  mm was calculated for different delamination lengths  $a$  using equation (5). The energy release rate decreases with increasing delamination length,  $a$ , as shown in Figure 5 (solid red circles and solid red line). Delamination growth was assumed to stop once the calculated energy release rate drops below the cutoff value,  $G_{th}$ , (green solid horizontal line). The static benchmark case (solid grey circles and dashed grey line in Figure 5), where the delamination propagates at constant  $G_{Ic}$  (solid blue line in Figure 5) was included for comparison.

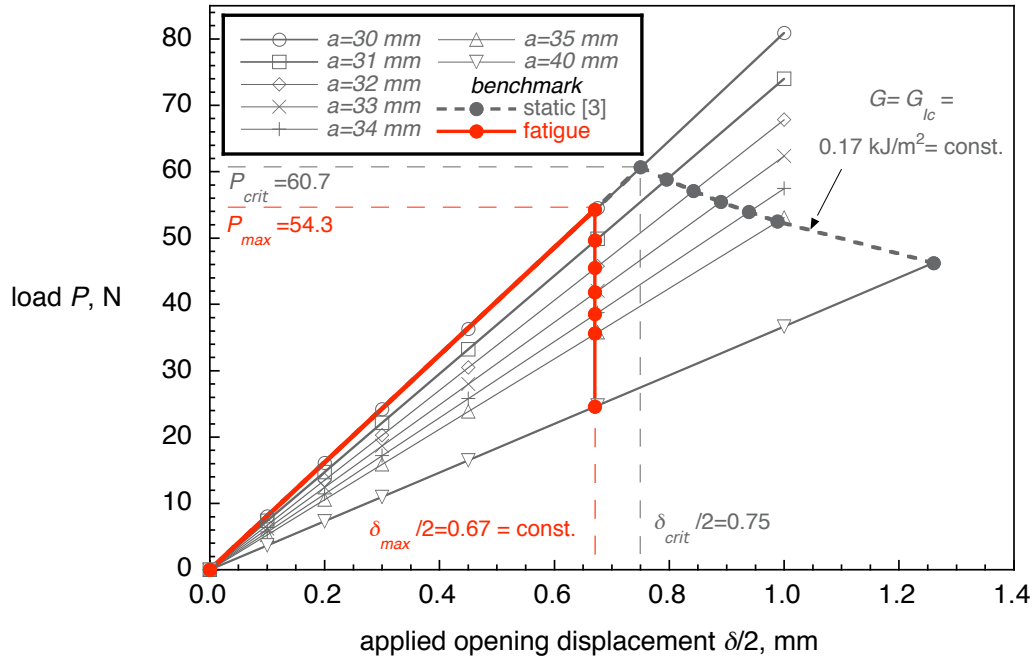


Figure 4. Critical load-displacement behavior for a DCB specimen.

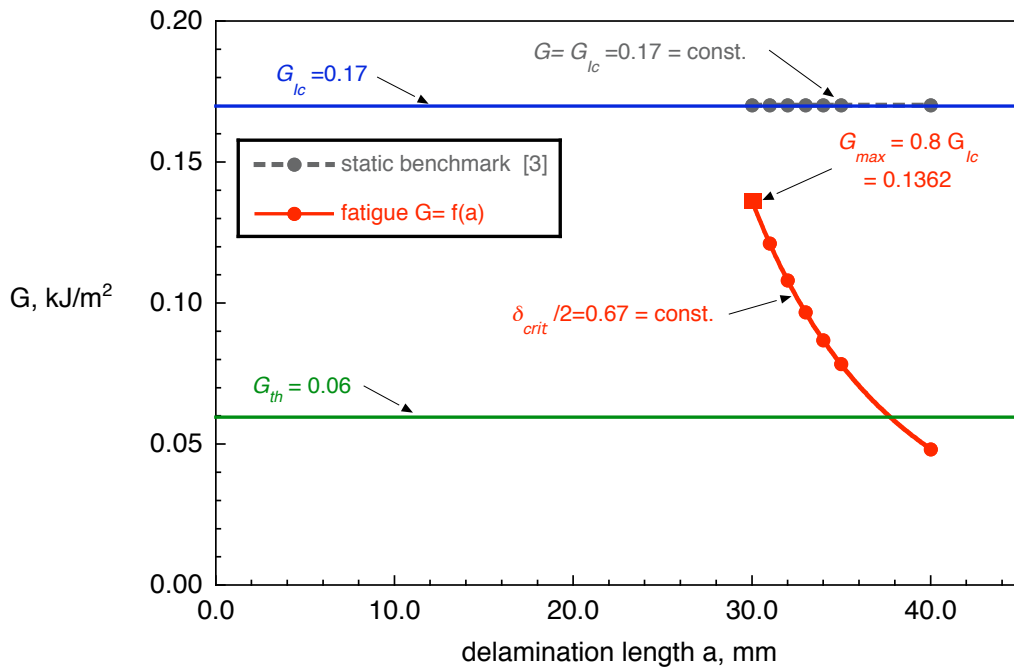


Figure 5. Energy release rate – delamination length behavior for DCB specimen.

A load ratio  $R=0.1$  was selected for this investigation as discussed in detail in reference 6. The corresponding minimum load,  $P_{min}$ , and minimum displacement,  $\delta_{min}/2$ , were calculated

$$R = \frac{P_{min}}{P_{max}} = \frac{\delta_{min}}{\delta_{max}} = 0.1 \Rightarrow \delta_{min} = 0.1 \cdot \delta_{max} \quad (6)$$

Further, a frequency  $f=10$  Hz was selected for this investigation as discussed in detail in reference 6.

In the analysis, the displacement  $\delta/2$  applied to each arm of the specimen is represented as a function of time,  $t$

$$\delta/2 = [a_0 + b_1 \cdot \sin \omega(t - t_0)] \cdot \delta_{max} / 2 \quad (7)$$

where  $\delta_{max}/2=0.67$  mm is the maximum displacement. The constants  $a_0=0.55$ ,  $b_1=0.45$ , the circular frequency  $\omega=20\pi=62.832$  and the starting time  $t_0=0.025$  are calculated from load ratio  $R=0.1$  and the frequency  $f=10$  Hz for testing.

## CREATING A BENCHMARK EXAMPLE FOR GROWTH PREDICTION

### Fatigue Delamination Growth Onset

The number of cycles to delamination onset,  $N_D$ , may be obtained by solving equation (1) for  $N_D$ .

$$G = m_0 \cdot N_D^{m_1} \Rightarrow N_D = \underbrace{\left(\frac{1}{m_0}\right)^{\frac{1}{m_1}}}_{c_1} \cdot G^{\frac{1}{m_1}} \Rightarrow N_D = c_1 \cdot G^{c_2} \quad (8)$$

where  $c_2 = \frac{1}{m_1}$ . Values for the constants  $c_1$  and  $c_2$  are shown in Figure 2.

At the beginning of the test, the specimen is loaded initially so that the energy release rate at the front,  $G_{Imax}$ , reaches about 80% of  $G_{Ic}$  corresponding to  $G_{Imax}=0.1362$  kJ/m<sup>2</sup> as shown in Figure 2 (horizontal dashed red line). From the delamination onset curve, the number of cycles to delamination onset is determined as  $N_D=150$  cycles (vertical dashed red line).

### Fatigue Delamination Growth

The number of cycles during stable delamination growth can be obtained by solving equation (2) for  $N_G$

$$N_G = \int dN = \int \frac{1}{c} G_{max}^{-n} \cdot da \quad (9)$$

As mentioned above, the specimen is loaded initially so that the energy release rate at the front,  $G_{I_{max}}$ , reaches about 80% of  $G_{Ic}$  corresponding to  $G_{I_{max}}=0.1362 \text{ kJ/m}^2$  in the current study as shown in the Paris Law plot of Figure 3 (solid red square).

For practical applications, equation (2) can be replaced by an incremental equivalent expression

$$\frac{\Delta a}{\Delta N} = c \cdot G_{\max}^n \quad (10)$$

where for the current study, increments of  $\Delta a=0.1 \text{ mm}$  were chosen. Starting at the initial delamination length  $a_0=30.5 \text{ mm}$ , the energy release rates  $G_{i,\max}$  were obtained for each increment,  $i$ , from the curve fit (solid red circles and solid red line) plotted in Figure 5. These energy release rate values were then used to obtain the increase in delamination length per cycle or growth rate  $\Delta a/\Delta N$  from the Paris Law in Figure 3. The growth rate rapidly decreases with increasing delamination length  $a$  as indicated by the red arrow in Figure 3. The number of cycles during stable delamination growth,  $N_G$ , was calculated by summing the increments  $\Delta N_i$

$$N_G = \sum_{i=1}^k \Delta N_i = \sum_{i=1}^k \frac{1}{c} G_{i,\max}^{-n} \cdot \Delta a \quad (11)$$

where  $k$  is the number of increments. The corresponding delamination length,  $a$ , was calculated by adding the incremental lengths  $\Delta a$  to the initial length  $a_0$ .

$$a = a_0 + \sum_{i=1}^k \Delta a = a_0 + k \cdot \Delta a \quad (12)$$

### Combined Fatigue Delamination Onset and Growth

For the combined case of delamination onset and growth, the total life,  $N_T$ , may be expressed as

$$N_T = N_D + N_G \quad (13)$$

where,  $N_D$ , is the number of cycles to delamination onset and  $N_G$ , is the number of cycles during delamination growth [9]. For this combined case, the delamination length,  $a$ , is plotted in Figure 6 for an increasing number of load cycles  $N_T$ . For the first  $N_D=150$  cycles, the delamination length remains constant (horizontal red line), followed by a growth section where - over  $N_G$  cycles - the delamination length increases following the Paris Law (crosses and solid red line). Once a delamination length is reached where the energy release rate drops below the assumed cutoff value,  $G_{th}$ , (as shown in the Paris Law in Figure 3) the delamination growth no longer follows the Paris Law (dashed grey line) and stops (horizontal solid red line).

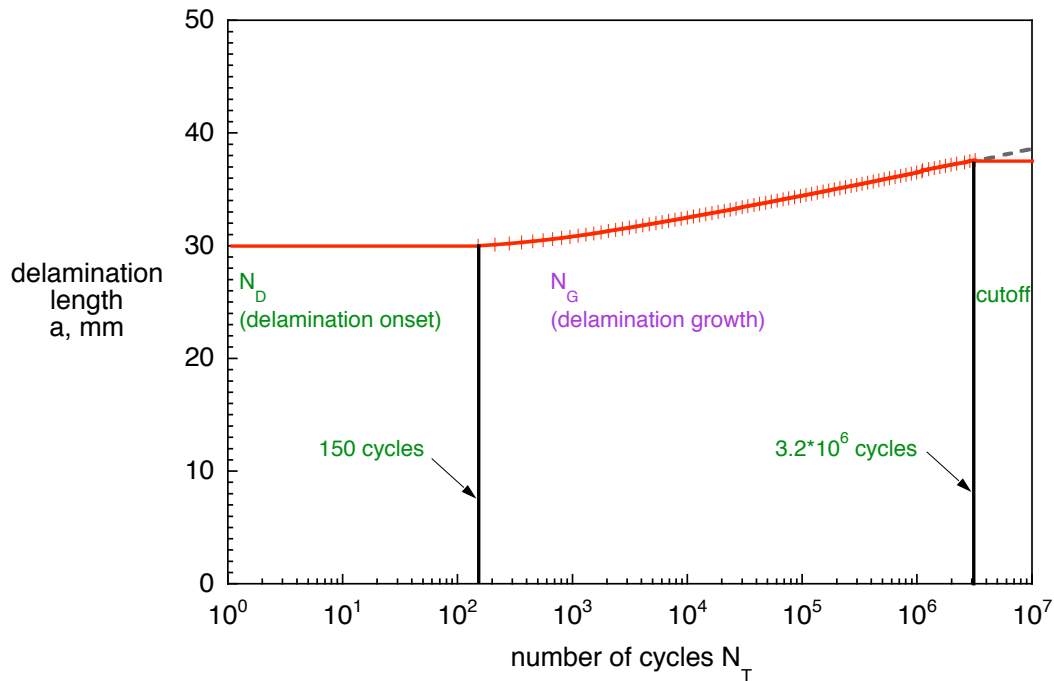


Figure 6. Delamination onset and growth behavior for DCB specimen.

## FINITE ELEMENT MODELING

A typical two-dimensional finite element model of a Double Cantilever Beam (DCB) specimen is shown in Figure 7a. The specimen was modeled with solid plane strain elements (CPE4) and solid plane stress elements (CPS4) in ABAQUS<sup>®</sup> Standard 6.8, 6.9 and 6.9EF. Along the length, all models were divided into different sections with different mesh refinement. The DCB specimen was modeled with six elements through the specimen thickness ( $2h$ ) as shown in the detail of Figure 7b. The resulting element length at the delamination tip was  $\Delta a = 0.5$  mm. A finer mesh, resulting in  $\Delta a = 0.25$  mm, was also generated. Additionally, three coarser meshes with a reduced number of elements in the length direction were also generated resulting in  $\Delta a = 1.0$  mm,  $\Delta a = 1.25$  mm and  $\Delta a = 1.67$  mm. The models are shown in reference 6.

The plane of delamination was modeled as a discrete discontinuity in the center of the specimen. For the analysis with ABAQUS<sup>®</sup> 6.8, 6.9 and 6.9EF, the models were created as separate meshes for the upper and lower part of the specimens with identical nodal point coordinates in the plane of delamination [10]. Two surfaces (top and bottom surface) were defined to identify the contact area in the plane of delamination as shown in Figure 7b. Additionally, a node set was created to define the intact (bonded nodes) region.

A typical three-dimensional finite element model of the DCB specimen is shown in Figure 7c. Along the length, all models were divided into different sections with different mesh refinement. A refined mesh was used in the center of the DCB specimen. Across the width, a uniform mesh was used to avoid potential problems at the transition between a coarse and finer mesh [3]. Through the specimen thickness ( $2h$ ), six elements were used. The resulting element length at the delamination tip was

$\Delta a=0.5$  mm. The specimen was modeled with solid brick elements (C3D8I) which had yielded excellent results in a previous studies [3]. Two coarser meshes with a reduced number of elements in the width and length directions, resulting in  $\Delta a=1.0$  mm and  $\Delta a=2.0$  mm, were also generated as shown in reference 6.

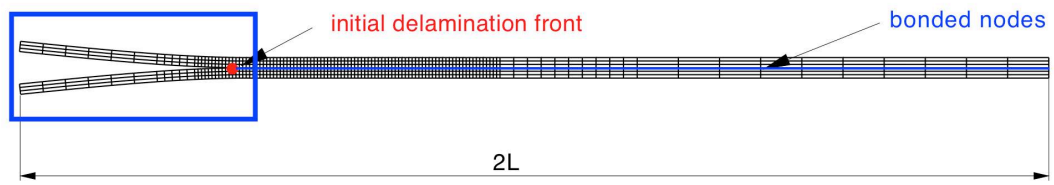
Three models of the DCB specimen were also generated with continuum shell elements (SC8R) resulting in an element length at the delamination tip  $\Delta a=0.5$  mm,  $\Delta a=1.0$  mm and  $\Delta a=2.0$  mm, respectively. In the  $z$ -direction, only one element was used to model the thickness of the specimen. These less-refined models were used to study the effect on performance (CPU time), computed load/displacement behavior and growth prediction in comparison with the more refined models discussed above. Details are discussed in reference 6.

For all the analyses performed, the low-cycle fatigue analysis in ABAQUS<sup>®</sup> Standard 6.8, 6.9 and 6.9EF was used to model delamination growth at the interfaces in laminated composites [10]. A direct cyclic approach is part of the implementation and provides a computationally effective modeling technique to obtain the stabilized response of a structure subjected to constant amplitude cyclic loading. Delamination onset and growth predictions are based on the calculation of the strain energy release rate at the delamination front using VCCT. To determine propagation, computed energy release rates are compared to the input data for onset and growth from experiments as discussed in the methodology section. During the analysis, at least one element length at the crack tip is released along the interface after each stabilized cycle [10].

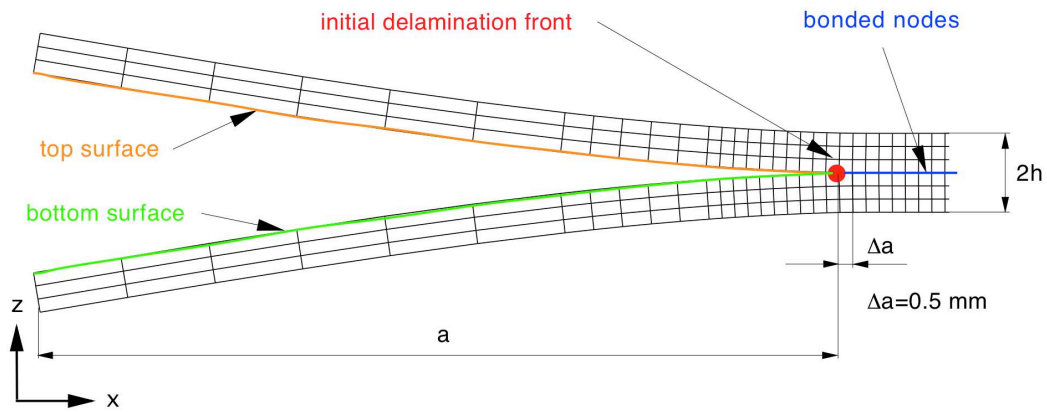
For all analyses, the elastic constants, the input to define the fracture criterion, and the parameters for delamination onset and delamination growth (Paris Law) were kept constant. The elastic constants, the fracture toughness values and the parameters required for delamination onset and growth are given in Table I. The parameters to define the load frequency ( $f=10$  Hz), the load ratio ( $R=0.1$ ) as well as the minimum and maximum applied displacement ( $\delta_{min}/2=0.067$  mm and  $\delta_{max}/2=0.67$  mm) were also kept constant during all analyses. To study the effect on the computed onset and growth behavior during the analysis:

- The number of terms used to define a Fourier series was varied. A Fourier series is used during the execution of the ABAQUS<sup>®</sup> Standard to approximate the periodic cyclic loading.
- The size of the initial time increment used in the analysis was varied.
- The input required to define the cyclic loading was altered.
- The release tolerance was varied. Once a user specified release tolerance ( $(G - G_c)/G_c > \text{release tolerance}$ ) is exceeded during the analysis in ABAQUS<sup>®</sup> Standard, a cutback operation is performed which reduces the time increment. The cutback reduces the degree of overshoot and improves the accuracy of the local solution.
- The solution controls were varied.

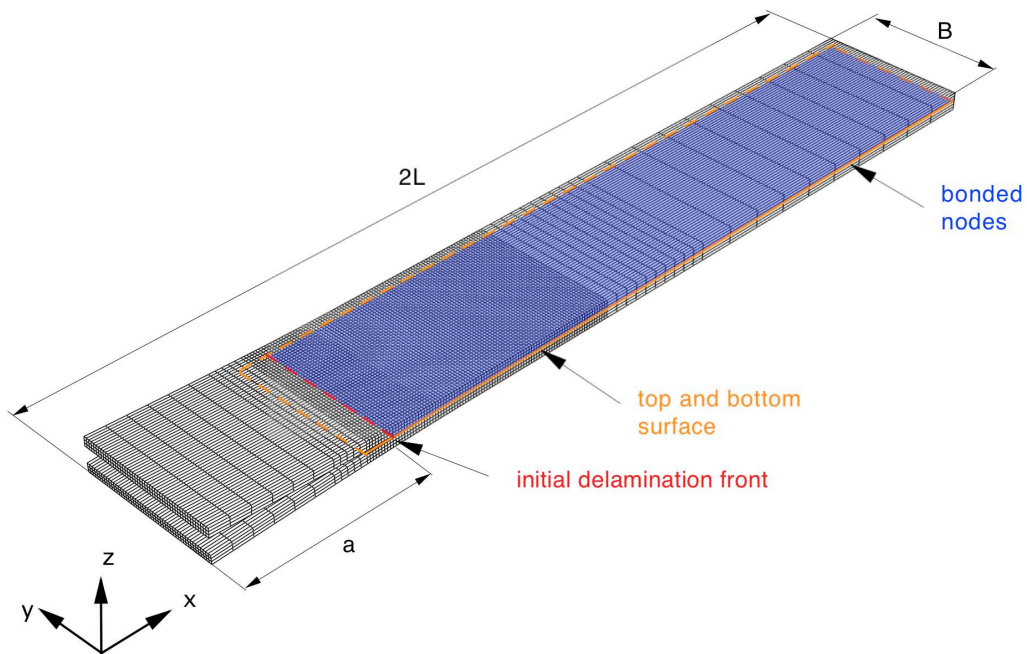
It was assumed that the computed onset and growth behavior should closely match the benchmark results established earlier. Setting the value of the input parameters correctly is often an iterative procedure, which will be discussed later. Further details about the required input parameters are discussed in reference 6 where sample input files are also provided.



a. Deformed two-dimensional FE-model of a DCB specimen with initial delamination



b. Detail of a deformed two-dimensional FE-model of a DCB specimen



c. Deformed three-dimensional FE-model of a DCB specimen with initial delamination front

Figure 7. Typical finite element models used in the simulations of delamination growth.

## ANALYSIS

### Results from Fatigue Onset and Growth Analysis

In Figures 8 to 14, the delamination length,  $a$ , is plotted versus the number of cycles,  $N$ , for different input parameters and models. For all results shown, the analysis stopped when a 10,000,000 cycles limit - used as input to terminate the analysis - was reached.

#### Initial Results

Initial results, as plotted in Figure 8, were obtained using the specified default values as input parameters (see appendix of reference 6). For better visualization of the results and to be able to identify the differences in the results, the scale on the vertical axis was expanded. The results obtained from two-dimensional plane strain (open blue circles and solid blue line) and plane stress (open red squares and solid red line) models as well as full three-dimensional models (open green diamonds and solid green line) were within 4% of the benchmark results (grey crosses and solid grey line). For all results shown, the predicted onset occurs prior to the benchmark result onset,  $N_D=150$  cycles. The onset value is lowest for the plane stress results, followed by the results obtained from 3D solid models and the plane strain results. This sequence can be explained by the computed energy release rate, where the values obtained from the plane stress model are slightly higher compared to the results obtained from 3D solid and plane strain models as discussed in reference 6. During the growth phase of the analysis, the results lie on curves with nearly the same slope parallel to the benchmark which suggests that the Paris Law was implemented correctly and is - as expected - independent of the model. For all models, the threshold cutoff, where delamination growth is terminated and the delamination length remains constant, is predicted close to the number of cycles defined by the benchmark.

#### Variation of Input Parameters

Input parameters were varied to study the effect on the computed onset and growth behavior during the analysis and results are plotted in Figures 9 and 10. For this parametric study, only models with a refined mesh ( $\Delta a=0.25$  mm) made of plane strain elements (CPE4) were used. Once a set of parameters was established that yielded good results, the effects of mesh size and element type on the results were studied.

First, the effect of the initial time increment used in the analysis settings was studied as shown in Figure 9 (see appendix of reference 6 for details). The initial time increment was varied between  $i_0=0.01$  (one tenth of a single loading cycle,  $t_s=0.1s$ , open blue circles and solid blue line) and  $i_0=0.0001$  (one thousandth of a single loading cycle, open green diamonds and solid green line). For larger initial time increments, the onset of delamination shifted towards a lower number of cycles. Reducing the initial time increments, however, significantly increased the computation time. Based on the results, it was therefore decided to use an initial time increment of  $i_0=0.001$  (open red squares and solid red line) for the remainder of the study to save computation time. This step is justified by the fact that the results

obtained for  $i_0=0.001$  were almost identical to the values obtained from the analysis where a smaller initial time increment was used ( $i_0=0.0001$ ).

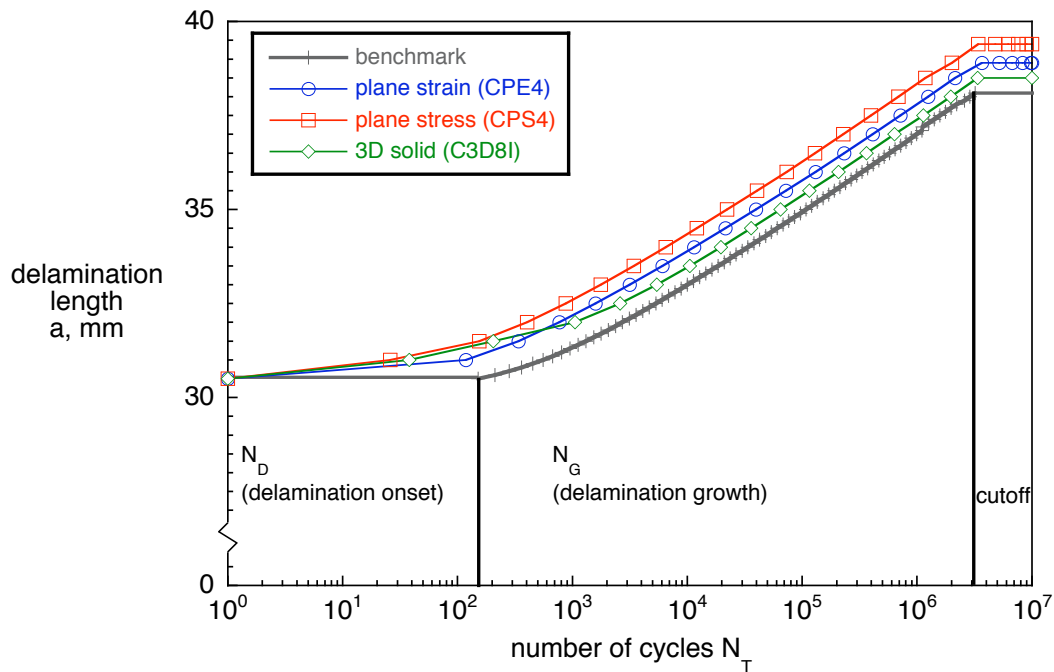


Figure 8. Computed delamination onset and growth: Detail of initial results.

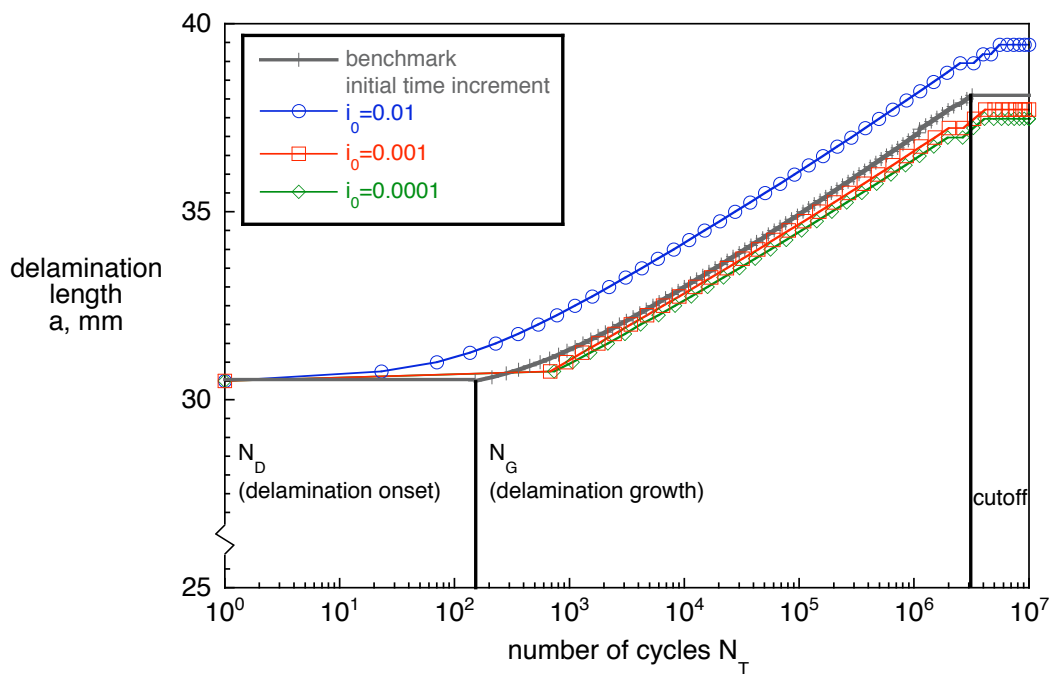


Figure 9. Computed delamination onset and growth obtained for different initial time increments.

Second, the input to define the cyclic loading was varied. In order to define the cyclic applied displacement,  $\delta/2$ , a set of parameters need to be determined as shown in the equation (7) and highlighted in Figure 10. Selecting  $A_1=0$  results in a sine curve representation of the cyclic load (analysis results are shown in Figure 10). Selecting  $B_1=0$  results in a cosine curve representation of the cyclic load. The selection of the starting time,  $t_0$ , causes a phase-shift. Further details about the input parameters are discussed in detail in the appendix of reference 6. As shown in Figure 10, the number of cycles to delamination onset is the most sensitive to input variations. The results obtained for the growth phase however, lie on curves with nearly the same slope, parallel to the benchmark. Also the threshold cutoff, where delamination growth is expected to stop and the delamination length remains constant, is predicted close to the number of cycles defined by the benchmark. A narrow band of results (green solid lines), was obtained when the number of terms used to define the Fourier series was increased to 50. A Fourier series is used in ABAQUS<sup>®</sup> Standard during the analysis to approximate the periodic cyclic loading (see appendix). The narrow band of results was in good agreement with the benchmark curve (grey solid line) compared to the results obtained for the default setting of 11 Fourier terms which showed more scatter (black dashed lines). It should be noted that one term in a Fourier series is sufficient to exactly represent a simple periodic function such as the simple sine function used in the current example. At the same time, a large number of terms should improve the approximation of a more complicated cyclic load as demonstrated. Good results could only be obtained when the analyses were performed with ABAQUS<sup>®</sup> Standard 6.9EF. Earlier versions showed unexplainable wide variations in results. The study was repeated for  $B_1=0$  which yielded similar results as discussed in detail in reference 6.

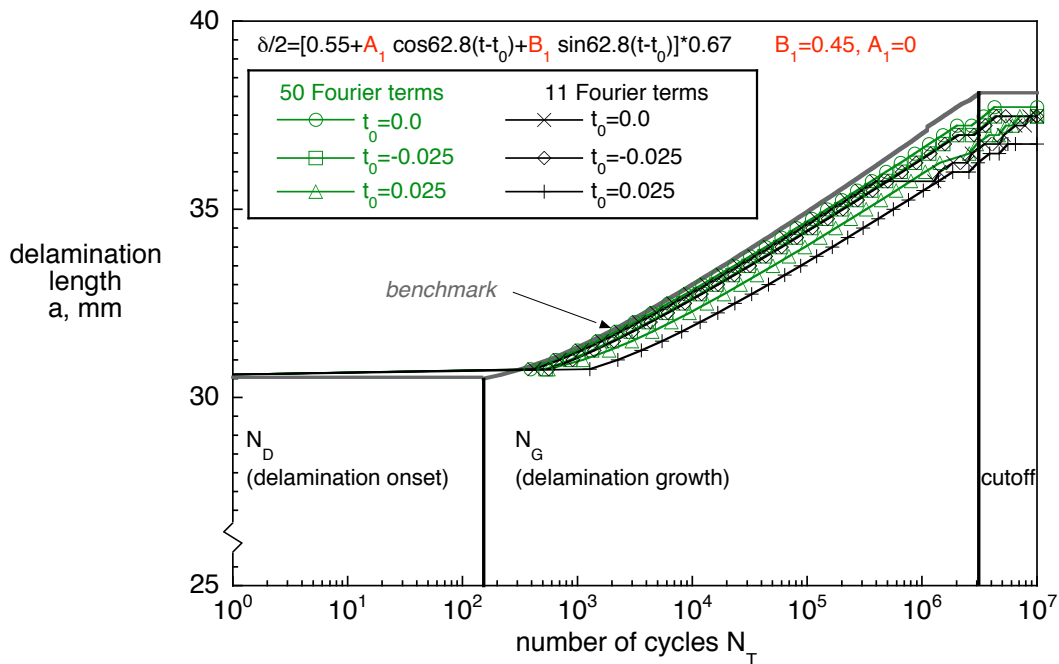


Figure 10. Computed delamination onset and growth obtained for sine representation of the cyclic loading.

Based on the current results, it was decided to use a sine curve representation ( $A_I=0$ ) in combination with the starting time,  $t_0=0.0$  for the remainder of the study.

Third, the release tolerance was varied. Once a user specified release tolerance ( $(G-G_c)/G_c > \text{release tolerance}$ ) is exceeded during the analysis in ABAQUS<sup>®</sup> Standard, a cutback operation is performed which reduces the time increment. The cutback reduces the degree of overshoot and improves the accuracy of the local solution [10]. In the current study, varying the input between 0.2 (the default value) and 0.01 did not have any effect on the computed onset and growth behavior during the analysis. It is assumed that the release tolerance only affects static delamination propagation and not growth under cyclic loading studied here.

Fourth, the solution controls were varied. It is generally not required nor recommended to modify the solution controls in ABAQUS<sup>®</sup> Standard. Since some of the solution controls, however, were modified in the DCB example problem provided with the ABAQUS<sup>®</sup> installation, it was decided to briefly address the effect on the computed onset and growth behavior during the analysis. The first input parameter that defines the iteration number at which the periodicity condition is first imposed, was not modified and the default value was kept. A series of analyses were performed where the other four input parameters were varied between 100 and  $10^{-4}$ . Changing the input did not have any effect on the computed onset and growth behavior during the analysis, however it significantly influenced the computation time. The analysis required only about a tenth of the computation time when the second input parameter was modified from the default value ( $5 \cdot 10^{-3}$ ) to values larger than  $10^{-1}$ . Changing the other remaining three parameters did not have any effect for this example. Further details about the input parameters are discussed in reference 6, where also sample input files are provided.

## Variation of Mesh Size and Element Type

The results obtained for models with different mesh sizes and different element types are shown in Figures 11 to 13. For models made of plane strain elements (CPE4), the element length,  $\Delta a$ , at the delamination tip was varied as discussed earlier. The results obtained from the respective models are plotted in Figure 11. Excellent agreement with the benchmark curve (grey crosses and grey solid line) could be achieved for element lengths up to  $\Delta a=1.25$  mm, as shown in Figure 11. For element length  $\Delta a=1.67$  mm (purple triangles and solid purple line), the predicted onset occurs for a slightly higher number of cycles. The observed mismatch is largely due to the increased element length, which causes the first growth step to be larger. The following growth increments are relatively large due to the increased element length ( $\Delta a=1.67$  mm). However, during the growth phase of the analysis, the results from all models lie on curves with the same slope parallel to the benchmark, which suggests that the Paris Law was implemented correctly and is, as expected independent, of the mesh. For all models, the threshold cutoff, where delamination growth is expected to stop and the delamination length remains constant, is predicted close to the number of cycles defined by the benchmark. The total computation time was between 70 s for the coarsest mesh and 1030 s for the finest mesh as shown in Figure 12<sup>1</sup>.

---

<sup>1</sup> CPU time on Dual-Core AMD Opteron(tm) Processor 8220 SE

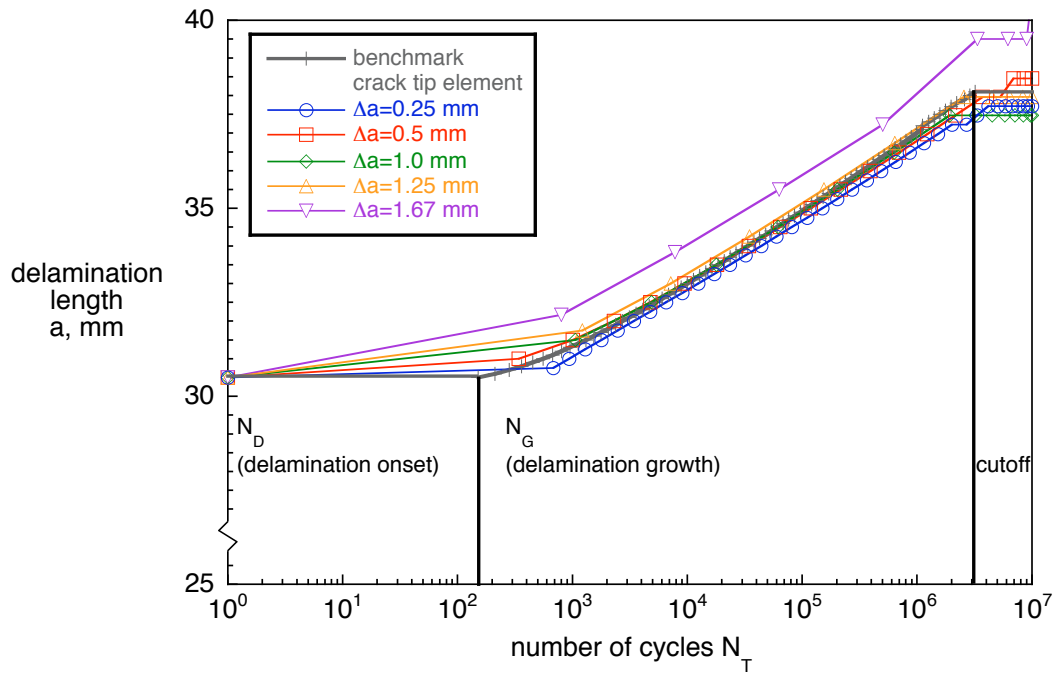


Figure 11. Computed delamination onset and growth behavior for different plane strain models.

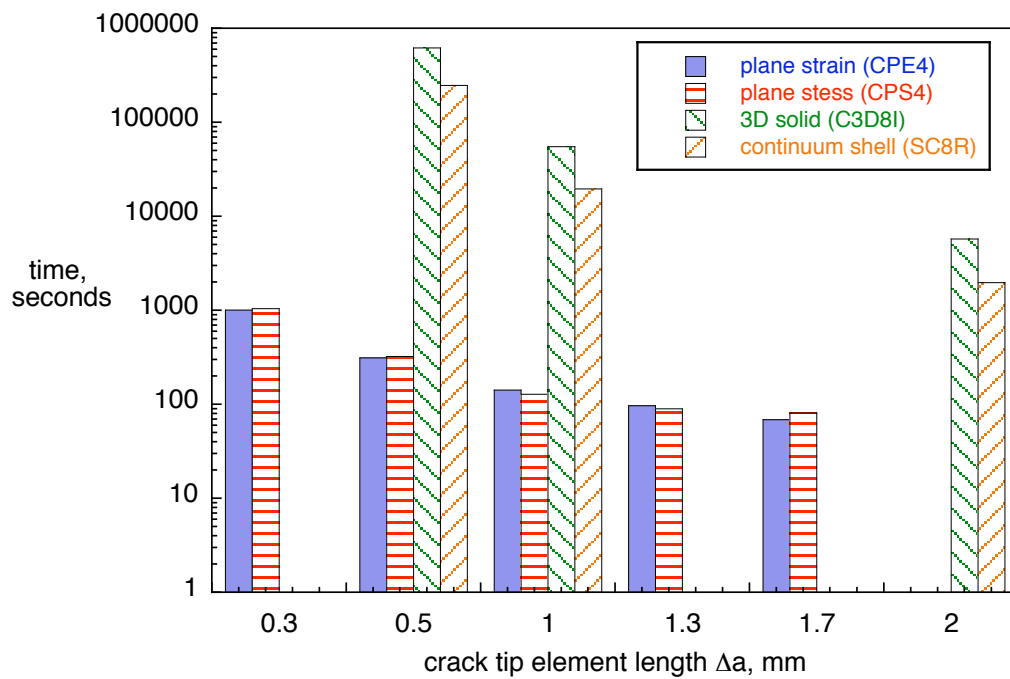


Figure 12. Required analysis time for models with different crack tip element lengths.

The analyses were repeated for models made of plane stress elements (CPS4), where the element length,  $\Delta a$ , at the delamination tip was varied as before. The results obtained from the respective models are discussed in reference 6. The computation times are included in Figure 12 for comparison.

The results obtained for models made of 3D solid and continuum shell elements showed the same trends and are discussed in detail in reference 6. The computational effort, however, was reduced by a factor of 2.5 to 2.9 for analyses performed using the continuum shell element models. For the models made of 3D solid elements, the total computation time was between 5800 s for the coarsest mesh and about 7 days for the finest mesh. For the corresponding models made of continuum shell elements, the total computation time was between 2000 s for the coarsest mesh and about 2.8 days for the finest mesh<sup>1</sup>. The computation times are also included in Figure 12 for comparison.

For final comparison, finite element analyses were repeated with two-dimensional and three-dimensional models with the same element length,  $\Delta a=0.5$  mm, at the delamination tip. The results obtained from two-dimensional plane strain (open blue circles and solid blue line) and plane stress (open red squares and solid red line) models as well as full 3D solid models (open green diamonds and solid green line) and continuum shell elements (orange x's and solid orange line) were within 1% of the benchmark curve (grey crosses and solid grey line) as shown in Figure 13. The results obtained from the continuum shell element model (orange x's and solid orange line) were almost identical compared to results obtained from the full 3D solid model (open green diamonds and solid green line) as mentioned above. The results obtained from plane stress models (open red squares and solid red line) are close to the results obtained from three-dimensional models.

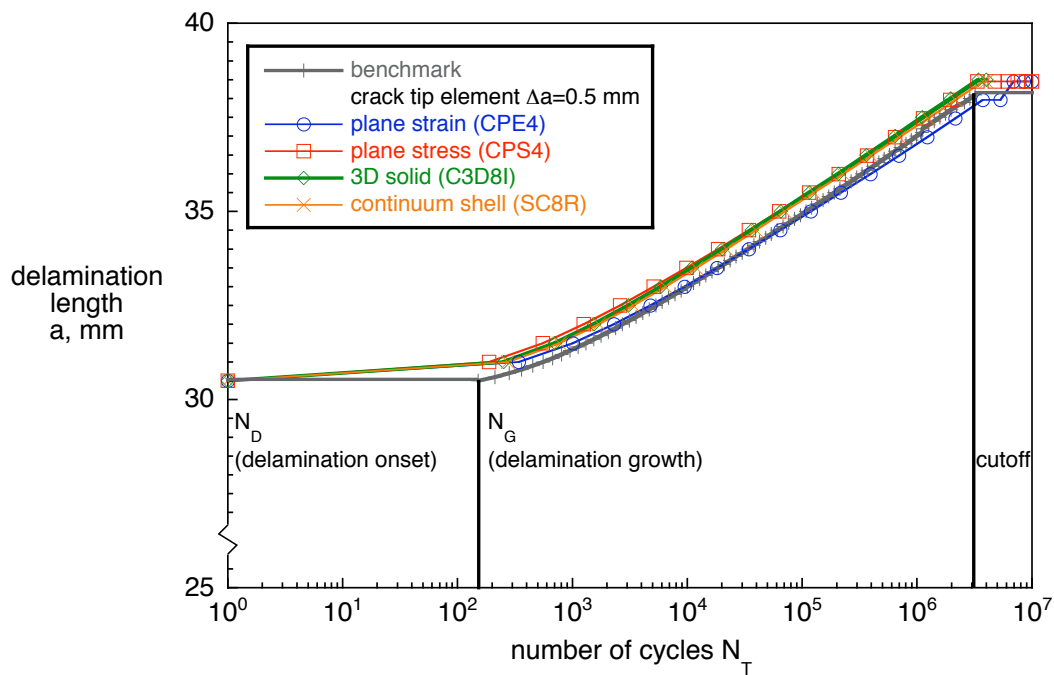


Figure 13. Computed delamination onset and growth behavior for different 2D and 3D models.

For all results shown, the predicted onset occurs first for the plane stress results and last for the plane strain results. Also, the delamination length obtained from plane strain models are slightly lower. This observation can be explained by looking at the computed energy release rate. The plane stress model yields a slightly higher energy release rate compared to the 3D solid and the plane strain model. Details are discussed in reference 6. Delamination onset would therefore occur first in plane stress models as indicated by the results plotted in Figure 13. During the stable growth phase, however, the results for all models lie on curves with nearly the same slope parallel to the benchmark as mentioned earlier. For all models, the threshold cutoff, where delamination growth is assumed to stop and the delamination length remains constant, is predicted close to the number of cycles defined by the benchmark.

## SUMMARY AND CONCLUSIONS

The development of a benchmark example for cyclic delamination growth prediction is presented and demonstrated for the commercial finite element code ABAQUS<sup>®</sup> Standard. The example is based on a finite element model of a Double Cantilever Beam (DCB) specimen, which is independent of the analysis software used and allows the assessment of the delamination growth prediction capabilities in commercial finite element codes. First, the development of a benchmark example for delamination fatigue growth prediction was presented step by step. The number of cycles to delamination onset was calculated from the material data for mode I fatigue delamination growth onset. The number of cycles during stable delamination growth was obtained incrementally from the material data for mode I fatigue delamination propagation. For the combined benchmark case of delamination onset and growth, the delamination length was calculated for an increasing total number of load cycles. Second, starting from an initially straight front, the delamination was allowed to grow under cyclic loading. The number of cycles to delamination onset and the number of cycles during stable delamination growth for each growth increment were obtained from the analysis.

The results showed the following:

- In general, good agreement between the results obtained from the growth analysis and the benchmark results could be achieved by selecting the appropriate input parameters. However, selecting the appropriate input parameters was not straightforward and often required an iterative procedure.
- The onset prediction appeared much more sensitive to the input parameters than the growth prediction.
- Consistent results were obtained when input parameters were selected such that 50 terms in the Fourier series were used during the execution of ABAQUS<sup>®</sup> Standard to approximate the periodic cyclic loading.
- Good agreement between analysis results and the benchmark could be achieved when the initial time increment used in the analysis was about one tenth of a single loading cycle.
- Best results were obtained when a sine curve representation of the cyclic applied displacement was selected in combination with the starting time,  $t_0=0.0$ .
- The release tolerance did not have an effect on the analysis or the results.

- Accurately computing the onset and growth required fine meshes with an element length at the tip  $\Delta a \leq 1.0$  mm.
- The solution controls in ABAQUS<sup>®</sup> Standard had to be modified in order to reduce computation time. Even with carefully selected input parameters, the analyses for three-dimensional models of a simple DCB specimen required days.
- Although implemented in ABAQUS<sup>®</sup> Standard 6.8, version 6.9EF was required to obtain consistently good results.
- Improvements are needed to make this analysis applicable to real case scenarios such as more complex specimens or structural components.

Overall, the results are promising. In a real case scenario, however, where the results are unknown, obtaining the right solution will remain challenging. Further studies are required which should include the assessment of the propagation capabilities in more complex mixed-mode specimens and on a structural level.

Assessing the implementation in one particular finite element code illustrated the value of establishing benchmark solutions since each code requires specific input parameters unique to its implementation. Once the parameters have been identified, they may then be used with confidence to model delamination growth for more complex configurations.

## ACKNOWLEDGEMENTS

This research was supported by the Aircraft Aging and Durability Project as part of NASA's Aviation Safety Program.

The analyses were performed at the Durability, Damage Tolerance and Reliability Branch at NASA Langley Research Center, Hampton, Virginia, USA.

## REFERENCES

1. E. F. Rybicki and M. F. Kanninen, "A Finite Element Calculation of Stress Intensity Factors by a Modified Crack Closure Integral," *Eng. Fracture Mech.*, vol. 9, pp. 931-938, 1977.
2. R. Krueger, "Virtual Crack Closure Technique: History, Approach and Applications," *Applied Mechanics Reviews*, vol. 57, pp. 109-143, 2004.
3. R. Krueger, "An Approach to Assess Delamination Propagation Simulation Capabilities in Commercial Finite Element Codes," NASA/TM-2008-215123, 2008.
4. I. S. Raju and T. K. O'Brien, "Fracture mechanics concepts, stress fields, strain energy release rates, delamination and growth criteria," in *Delamination behavior of composites*, S. Sridharan, Ed.: Woodhead Publishing in Materials, 2008.
5. "ASTM D 5528-01, Standard Test Method for Mode I Interlaminar Fracture Toughness of Unidirectional Fiber-Reinforced Polymer Matrix Composites," in *Annual Book of ASTM Standards*. vol. 15.03: American Society for Testing and Materials, 2008.
6. R. Krueger, "Development of a Benchmark Example for Delamination Fatigue Growth Prediction," NIA Report No. 2010-04, 2010.
7. "ASTM D 6115-97, Standard Test Method for Mode I Fatigue Delamination Growth Onset of Unidirectional Fiber-Reinforced Polymer Matrix Composites," in *Annual Book of ASTM Standards*. vol. 15.03: American Society for Testing and Materials, 2008.
8. P. Hansen and R. Martin, "DCB, 4ENF and MMB Delamination Characterisation of S2/8552 and IM7/8552," Materials Engineering Research Laboratory Ltd. (MERL), Hertford, UK N68171-98-M-5177, 1999.
9. "Fatigue Fracture Toughness," in *Composite Materials Handbook CMH-17*. Rev. G, Vol. 1 , section 6.9.4, ASTM International, 2010.
10. Abaqus Analysis User's Manual, ABAQUS<sup>®</sup> Standard, Version 6.9, DSS Simulia, 2009.